MICS JOURNAL Mathematics-in-Industry Case Studies Journal, Volume 2, pp. 155-173 (2010)

Determination of the index of refraction of anti-reflection coatings

D. Lesnic * G. Wakefield † B.D. Sleeman ‡ J.R. Ockendon §

Abstract. In this paper we investigate the inverse determination of a space-wise dependent index of refraction of a dielectric obstacle. Such a dielectric specimen could be an optical anti-reflection coating structure as is used in various optical instruments. The mathematical model is based on solving an inverse coefficient identification problem for the one-dimensional Helmholtz equation. The numerical method and solution are first validated in terms of accuracy and stability for a benchmark test example, after which the technique is applied to a case study concerning inverting real experimentally measured reflectance data supplied by Oxford Advanced Surfaces Ltd. A better fit to the data is obtained when a continuous index of refraction is sought, rather than a piecewise constant function, as in previous studies.

Keywords. Index of refraction, Anti-reflection coatings, Reflection coefficient.

1 Introduction

In recent years, anti-reflection coatings (ARC's) have become a key and vital feature for high-efficiency silicon solar cell design, see [24], [12], and the review by [4]. They are also widely used to increase transmission and reduce glare resulting from window coatings in a diverse range of industries such as photovoltaics, buildings, displays, and opthalmics. ARC's currently in use enhance the transparency of certain surfaces by the introduction of a smooth and gradual change in effective refractive index between two media, see Figure 1. This results in improved efficiency of some commercial architectural glazing and solar collectors. As a possible alternative technology, much can be learnt from optical biomimetics by looking at the antireflective optical nanostructures found in insect eyes; unfortunately, antireflection has not yet benefitted from such a technology transfer, see [25].

*University of Leeds, Department of Applied Mathematics, Leeds LS2 9JT, UK, amt5ld@maths.leeds.ac.uk

†Oxford Advanced Surfaces Group Plc, Oxford University, Begbroke Science Park, Sandy Lane, Yarnton OX5 1PF, UK, gareth.wakefield@oxfordsurfaces.com

‡University of Leeds, Department of Applied Mathematics, Leeds LS2 9JT, UK, bds@maths.leeds.ac.uk

§Oxford Centre for Industrial and Applied Mathematics, Mathematical Institute, 24-29 St Giles', Oxford OX1 3LB, UK, ock@maths.ox.ac.uk

In the simplest setting, the reflection from any given interface at normal incidence is related to the ratio of refractive indices of the materials forming the interface and is characterised by the % reflectance given by $100(n_0 - n_s)^2/(n_0 + n_s)^2$, where n_0 is the refractive index of the first layer (air) and n_s is the refractive index of the second layer (window), see [27] and [12]. Thus, for a crown glass window, $n_0 = 1$ and $n_s = 1.52$ giving a reflectance at normal incidence of 4.3% per surface, i.e. a total reflectance of 8.6% from the window. In order to minimize or remove this reflectance completely a further layer of refractive index n_1 is coated onto the window such that reflections from the air/coating and coating/window interfaces undergo destructive interference to the greatest possible extent. In this case, for a certain wavelength λ related to the film thickness d, namely if $\lambda = 4dn_1$, and if $n_1 = \sqrt{n_0 n_s}$, see [27] and [12] and later on Example 4.1 of Section 4, it is possible that the reflection becomes zero. Thus, for example, at a normally incident wavelength of $550nm$ (green light) a perfect ARC on a crown glass window will have a thickness of $112nm$ and a refractive index of 1.23. However, this assumes that the refractive index is constant throughout the thickness of the coating. If the experimental reflectivity curves deviate from those predicted by this simplified homogeneous single layer model this is indicative of some refractive index gradient within the film. However, there is no way to measure this gradient directly. The gradient is important as it provides useful information regarding the relationship between the optical and mechanical properties of the ARC.

In the optical coating synthesis problem, the unknown refractive index is varied in space, either continuously or piecewise, so as to approximate the spectral characteristics, such as the transmission or reflection coefficient, with the desired accuracy. The solution of this problem in turn can then be used to optimize the design of optical coatings. The difficulty in solving this inverse problem comes from the fact that it is ill-posed; for example, the solution may be non-unique and widely different refractive indices may have close spectral characteristics, or the solution may be unstable, i.e. small errors in the spectral characteristics measurements can cause large errors in the retrieved refractive index.

2 Mathematical Formulation

In this section we formulate a class of inverse scattering problems in one dimension for the determination of index of refraction of a scatterer, i.e. the optical coating, from scattering data, i.e. the reflection coefficient.

Consider the wave refraction propagation initiated by a transverse wave in which the electric and magnetic fields are at right angles to each other, and to the direction of propagation which is taken as the $x-$axis, incident from $x = -\infty$ of the form $u_{inc}(x) = e^{ikn_0 x}$, where $k = \omega/c$ is the free-space wavenumber, ω is the frequency, $c = 1/\sqrt{\epsilon_0 \mu_0}$ is the speed of light, ϵ_0 and μ_0 are the permittivity and magnetic permeability of the air free-space, respectively, $n_0 = 1$ is the refractive index of the outside air environment. The wave impinges on a dielectric graded-index obstacle of

known thickness $d > 0$ and unknown refractive index $n(x)$, in contact with an infinitely thick glass substrate absorbing material of uniform index of refraction $n_s = 1.52$, see Figure 1 for $\theta = 0$ angle of incidence. Upon imposing the continuity at the interfaces $x = 0$ and $x = d$, from the time-

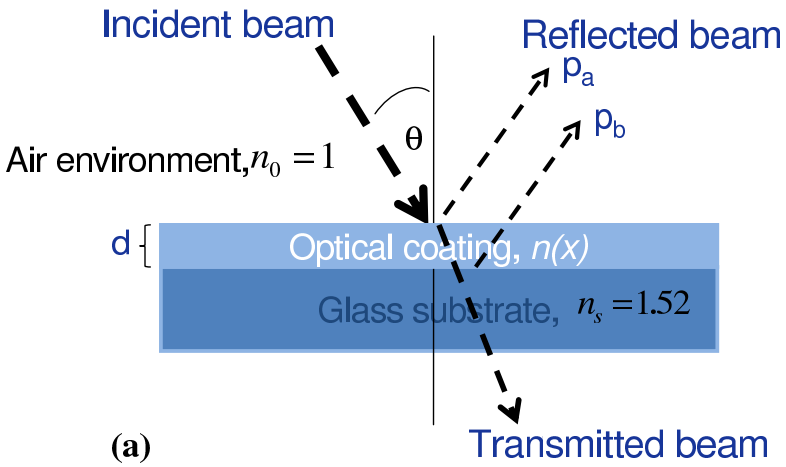

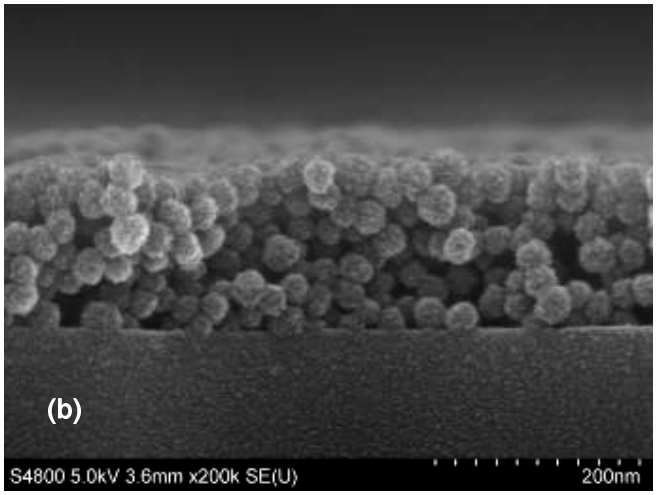

Figure 1: *(a) A schematic diagram of an anti-reflection coating of thickness d. When p_a and p_b are an angle of π out of phase and have equal amplitude, the magnitude of the reflected wave is zero. (b) An electron micrograph of a cross section of an anti-reflection coating on glass.*

harmonic Maxwell's equations one obtains that the y-component $u(x)$ of the electric field satisfies

the following second-order, non-dimensionalised, boundary value problem, see [8],

$$u''(x) + \beta^2 \epsilon(x) u(x) = 0, \quad x \in (0,1), \tag{1}$$

$$u'(0) + i n_0 \beta u(0) = 2 i n_0 \beta, \tag{2}$$

$$u'(1) - i n_s \beta u(1) = 0, \tag{3}$$

where $\epsilon(x) = n^2(x)$ is the dielectric permittivity of the optical coating, $\beta = kd = 2\pi d/\lambda$ is the non-dimensionalised wavenumber, and λ is the wavelength. We wish to solve the inverse problem of determining $\epsilon(x)$ (and hence $n(x) = \sqrt{\epsilon(x)}$) from the reflection coefficient measurements

$$R(\beta) := u(0) - 1, \quad \text{for } \beta \in [\beta_{min}, \beta_{max}]. \tag{4}$$

One could also attempt to measure the transmission coefficient

$$T(\beta) := u(1) e^{-i n_s \beta}, \quad \text{for } \beta \in [\beta_{min}, \beta_{max}], \tag{5}$$

in addition to (4), but this additional information will not be considered in this study as it is not available yet from practical measurements. We remark that from (2) and (4) we have

$$u(0) = 1 + R(\beta), \quad u'(0) = i n_0 \beta (1 - R(\beta)), \tag{6}$$

thus, one can recast the boundary value problem (1)-(4) as an initial value problem (1), (3) and (6).

The problem given by equations (1)-(4) is an ordinary inverse coefficient identification problem, see [7], which is nonlinear and ill-posed, i.e. the solution may not exist, may not be unique, or it may not depend continuously on the input data (4). First, concerning the existence of a solution, a coating that realises the given reflection coefficient $R(\beta)$ for all values of $\beta \in [\beta_{min}, \beta_{max}]$ does not necessarily exist. Hence, the additional noisy measurement (4) should be understood in a least-squares sense which minimizes, with respect to $n \in N_{ad} := \{n \in L_\infty(0,1) \mid n_0 \le n(x) \le n_s, \forall x \in (0,1)\}$, the functional $F : N_{ad} \to \mathbb{R}_+$ defined by

$$F(n) := \| R(\beta) + 1 - u(0; \beta, n) \|^2_{L_2[\beta_{min}, \beta_{max}]}. \tag{7}$$

Second, concerning the uniqueness of the solution, different coatings may produce the same given reflection coefficient $R(\beta)$ for $\beta \in [\beta_{min}, \beta_{max}]$. It is unclear whether (i) the finite range $[\beta_{min}, \beta_{max}]$ is sufficient for uniqueness, i.e., should the reflection coefficient $R(\beta)$ be known for all positive wavenumbers $\beta \in (0, \infty)$ or, whether uniqueness of the solution still holds if only the reflectance $|R(\beta)|$, i.e. the magnitude of the complex reflection coefficient $R(\beta)$, is measured as

$$|R(\beta)| = |u(0) - 1|, \quad \text{for } \beta \in [\beta_{min}, \beta_{max}]. \tag{8}$$

A more detailed study of the uniqueness of solution will be described in the next section. Third, concerning stability, small errors which are inherently present in the practical measurements (4),

or (8), may cause large errors in the desired index of refraction. In order to prevent unphysical unstable solutions, regularization methods have to be applied, using some prior information about the behaviour of $n(x)$. This may include physical bounds such as $n \in N_{ad}$ and the continuity (or smoothness) of the function $n(x)$ which is imposed by adding to the least-squares function (7) a penalty regularization term. Hence, we will minimize the Tikhonov regularization functional

$$F_\Lambda(n) := \|R(\beta) + 1 - u(0;\beta,n)\|^2_{L_2[\beta_{min},\beta_{max}]} + \Lambda\|n - n^*\|^2_{L_2(0,1)}, \tag{9}$$

where $n^*(x) \in [n_0, n_s]$ is an *a priori* guess of the solution $n(x)$ and $\Lambda \geq 0$ is a regularization parameter which needs to be prescribed, for example using the so-called L-curve criterion. According to this criterion, the regularization parameter $\Lambda > 0$ can be chosen at the corner of the "L-curve" generated by plotting the solution norm $\|n - n^*\|_{L_2(0,1)}$ against the residual norm $\|R(\beta)+1-u(0;\beta,n)\|_{L_2[\beta_{min},\beta_{max}]}$ for a range of values of Λ. Despite some limitations, see [14], the L-curve has gained attention in recent years for practical computing of the selection of regularization parameters, see [15]. It will be employed to choose the regularization parameter Λ in Example 4.2 of Section 4. A more rigorous choice of the regularization parameter Λ, based on the *a priori* knowledge of the amount of noise with which the input data is contaminated, is discussed in more detail in Example 4.1 of Section 4.

The case of multilayer dielectric systems in which the reflection at the main contact surface is decreased due to the interference of the reflected light from each interface, so that the refractive index $n(x)$ is an unknown piecewise constant function, has been investigated in [27] (single and double layer), [19] (triple layer), and [7] (N layers). Although multilayer systems combined with surface texturization can reduce reflection losses to a few percent over the useful solar spectrum and thus improving the device performance and efficiency, see Ruby *et al.* (2002), the cost rapidly becomes higher.

Another practical manner in which to minimize reflection is to deposit an inhomogeneous dielectric with a gradual decrease of refractive index from the glass substrate to the ambient air, see [17]. Thus, the spacewise variation of $n(x)$ through the depth of the rugate film is continuous, in contast to the classical multilayer stacks, see [16]. In the literature, it is reported that coatings with a smooth continuous variation of the refractive index, compared with classical multilayer stacks, show higher laser induced damage threshold, see [21], less scattering losses and better optical properties, see [16].

The identification of a continuous refractive index has been investigated by various methods, for e.g. the Gelfand-Levitan-Marchenko spectral method, see [2], the integral equation method, see [13], the spline approximation projection method, see [9], techniques based on trace formulae, see [5], the low-coherence interferometric imaging, see [3], techniques based on coupled-mode Zakharov-Shabat equations, see [11], [26], [1].

Concerning design, not every coating system is realisable in practice, e.g. manufacturing constraints may impose restrictions on the characteristics of the available materials.

3 Uniqueness of Solution

In this section we analyse in more detail the inverse medium diffraction problem (1)-(4), or equivalently (1), (3) and (6), under the key assumption that we know the reflection coefficient $R(\beta)$ for all values of $\beta \in (0, \infty)$. We will now describe the formulation of the problem as an inverse scattering problem. We employ the well-known ansatz, see [1],

$$\begin{aligned} u(x) &= \tfrac{1}{\sqrt{\beta n(x)}} \left(A(x) e^{iS(x)} + B(x) e^{-iS(x)} \right), \\ u'(x) &= i\sqrt{\beta n(x)} \left(A(x) e^{iS(x)} - B(x) e^{-iS(x)} \right), \end{aligned} \tag{10}$$

where $S(x) = \beta \int_0^x n(\zeta) d\zeta$. For eqn.(10) to hold we must have

$$\begin{aligned} &i\sqrt{\beta n(x)} \left(A(x) e^{iS(x)} - B(x) e^{-iS(x)} \right) = u'(x) = -\tfrac{n'(x)}{2\sqrt{\beta n^3(x)}} \left(A(x) e^{iS(x)} + B(x) e^{-iS(x)} \right) \\ &+ \tfrac{1}{\sqrt{\beta n(x)}} \left[(A'(x) + i\beta n(x) A(x)) e^{iS(x)} + (B'(x) - i\beta n(x) B(x)) e^{-iS(x)} \right]. \end{aligned} \tag{11}$$

This is ensured if we choose

$$A'(x) = \frac{n'(x)}{2n(x)} B(x) e^{-2iS(x)}, \quad B'(x) = \frac{n'(x)}{2n(x)} A(x) e^{2iS(x)}. \tag{12}$$

Assuming that $n \in C[0,1]$ is continuous function on $[0,1]$, in particular we have $n(0) = n_0$ and $n(1) = n_s$, and then the boundary conditions (2) and (3) yield

$$A(0) = \sqrt{\beta n_0}, \quad B(1) = 0. \tag{13}$$

Also, in terms of the reflection coefficient, condition (6) gives

$$B(0) = R(\beta)\sqrt{\beta n_0}. \tag{14}$$

Now define

$$P(x) = A(x) e^{iS(x)}, \quad Q(x) = B(x) e^{-iS(x)}. \tag{15}$$

Differentiating (15) and using (12) we obtain

$$P'(x) = i\beta n(x) P(x) + \frac{n'(x)}{2n(x)} Q(x), \quad Q'(x) = -i\beta n(x) Q(x) + \frac{n'(x)}{2n(x)} P(x). \tag{16}$$

The boundary conditions (13) and (14) give

$$P(0) = \sqrt{\beta n_0}, \quad Q(0) = R(\beta)\sqrt{\beta n_0}, \quad Q(1) = 0. \tag{17}$$

Writing the optical path length as

$$\xi(x) = \frac{S(x)}{\beta} = \int_0^x n(\zeta) d\zeta, \tag{18}$$

eqns.(16) become the Zakharov-Shabat system

$$\dot{P} = qQ + i\beta P, \quad \dot{Q} = qP - i\beta Q, \tag{19}$$

where the dot denotes the differentiation with respect to ξ, and the coupling coefficient is given by

$$q(\xi) = \frac{\dot{n}(\xi)}{2n(\xi)} = \frac{d}{d\xi}\left(log(\sqrt{n(\xi)})\right). \tag{20}$$

The boundary conditions associated to (19), from (17), are

$$P(0) = \sqrt{\beta n_0}, \quad Q(0) = R(\beta)\sqrt{\beta n_0}, \quad Q(\overline{n}) = 0, \tag{21}$$

where the average quantity

$$\overline{n} = \xi(1) = \int_0^1 n(\zeta)d\zeta \tag{22}$$

is called the full optical path length. Note that since $n > 0$, the function $\xi(x)$ is strictly increasing and thus $0 \leq \xi(x) \leq \overline{n}$ for all $x \in [0, 1]$. Upon dividing by $\sqrt{\beta n_0}$ in eqn.(21), the resulting problem given by eqns.(19) and (21) is precisely the problem P_2 discussed by [22]. It is well-known, see e.g. [2], that retrieving the real potential $V(\xi) = \dot{q}(\xi) + q^2(\xi)$ from the (left hand) reflection coefficient $\{R(\beta)|\beta \in \mathbb{R}\}$ is unique. Further, it can be shown that the real $q(\xi)$ is uniquely determined from standard results of the inverse scattering method, see e.g. [6]. Finally, if the function $q(\xi)$ is known, we can find the refractive index from eqn.(20) and the original coordinate x from eqn.(18), using the inversion formulae

$$n(\xi) = n_0\, exp\left[2\int_0^\xi q(\zeta)d\zeta\right], \quad x = \int_0^\xi \frac{d\zeta}{n(\zeta)}. \tag{23}$$

4 Numerical Implementation

In eqn.(1), the component of the electric field u is a complex function

$$u = A + iB, \tag{24}$$

where A and B are real. Substituting (24) into (1)-(3) we obtain

$$A''(x) + \beta^2\epsilon(x)A(x) = 0, \quad B''(x) + \beta^2\epsilon(x)A(x) = 0, \quad x \in (0, 1), \tag{25}$$

$$A'(0) - n_0\beta B(0) = 0, \quad B'(0) + n_0\beta A(0) = 2n_0\beta, A'(1) + n_s\beta B(1) = 0, \tag{26}$$

$$B'(1) - n_s\beta A(1) = 0. \tag{27}$$

Note that from (4)

$$R(\beta) = u(0) - 1 = A(0) - 1 + iB(0) = |R(\beta)|exp(i\ arg(R(\beta)))$$
$$|R(\beta)| = \sqrt{(A(0) - 1)^2 + B^2(0)}, \quad arg(R(\beta)) = tan^{-1}\left(\frac{B(0)}{A(0) - 1}\right). \tag{28}$$

We employ a central finite-difference method numerical discretisation of the eqns. (25)-(27) Let $x_j = j/N$ for $j = \overline{0,N}$ (the overlined notation $j = \overline{0,N}$ is used for $0 \leq j \leq N$ or $j = 0, 1, ..., N$ throughout), be a uniform discretisation of the interval $[0,1]$ with the mesh size $h = 1/N$. Denote $a_j = A(x_j)$, $b_j = B(x_j)$, $\epsilon_j = \epsilon(x_j)$ for $j = \overline{0,N}$. Then eqns. (25)-(27) in discretised form are given by

$$\frac{a_1 - a_{-1}}{2h} - n_0\beta b_0 = 0, \quad \frac{a_{j+1} - 2a_j + a_{j-1}}{h^2} + \beta^2\epsilon_j a_j = 0, \quad j = \overline{0,N},$$
$$\frac{a_{N+1} - a_{N-1}}{2h} + n_s\beta b_N = 0, \tag{29}$$

$$\frac{b_1 - b_{-1}}{2h} + n_0\beta b_0 = 2n_0\beta, \quad \frac{b_{j+1} - 2b_j + b_{j-1}}{h^2} + \beta^2\epsilon_j b_j = 0, \quad j = \overline{0,N},$$
$$\frac{b_{N+1} - b_{N-1}}{2h} - n_s\beta a_N = 0, \tag{30}$$

where a_{-1}, a_{N+1}, b_{-1} and b_{N+1} are fictitious values introduced in order to approximate using central finite differences the Robin boundary conditions (26) and (27). Equations (29) and (30) form a system of $(2N+6)$ equations with $(2N+6)$ unknowns, namely

$$(a_{-1}, a_0, a_1, ..., a_N, a_{N+1}, b_{-1}, b_0, b_1, ..., b_N, b_{N+1}),$$

if $\underline{\epsilon} = (\epsilon_0, \epsilon_1, ..., \epsilon_N)$ were known. However, in the inverse problem under investigation $\underline{\epsilon}$ is unknown, and it has to be inferred from some additional information. In practical measurements, the reflection coefficient $R(\beta)$ is usually measured for $M \geq N+1$ wavenumber (or wavelength) values

$$\beta_l = \frac{2\pi d}{\lambda_l} = \beta_{min} + \frac{(l-1)}{(M-1)}(\beta_{max} - \beta_{min}), \quad l = \overline{1,M}. \tag{31}$$

Let us denote these practical measurements by $R_l := R(\beta_l)$ for $l = \overline{1,M}$. From a given initial guess $\epsilon^*(x)$ for $\epsilon(x)$, we solve $M-$times the direct problem (29) and (30) to provide the complex values of the reflection coefficients $u(0;\beta_l,\underline{\epsilon}) - 1$ for $l = \overline{1,M}$. We then compare these computed reflection coefficients with the measured ones R_l and minimize iteratively the least-squares difference between them. Corresponding to (9) we have the following discretised functional to minimize $F_\Lambda : [n_0^2, n_s^2]^{N+1} \to \mathbb{R}_+$ defined by

$$F_\Lambda(\underline{\epsilon}) = \sum_{l=1}^{M} |u(0;\beta_l,\underline{\epsilon}) - 1 - R_l|^2 + \Lambda \sum_{j=0}^{N} (\epsilon_j - \epsilon_j^*)^2, \tag{32}$$

where $\underline{\epsilon}^* = (\epsilon_j)_{j=\overline{0,N}} \in [n_0^2, n_s^2]^{N+1}$ is an *a priori* guess of the solution $\epsilon(x)$. If the practical measurements are limited to the absolute value (magnitude) of the reflection coefficient, i.e. the amplitude, also called the square root of reflectance or the energy reflection coefficient, then instead of (32) we minimize the functional

$$\tilde{F}_\Lambda(\underline{\epsilon}) := \sum_{l=1}^{M} ||u(0;\beta_l,\underline{\epsilon}) - 1| - |R_l||^2 + \Lambda \sum_{j=0}^{N} (\epsilon_j - \epsilon_j^*)^2. \tag{33}$$

The minimization of (33) contains obviously less information than the minimization of (32).

The minimization of the functionals F_Λ (or $\tilde{F}_\Lambda$) defined by eqn.(32) (or eqn.(33)), subject to the simple physical bounds on the variables $1 = n_0^2 \leq \epsilon_j \leq n_s^2 = 2.3104$ for $j = \overline{0, N}$, is performed using the NAG Fortran routine E04JYF. This routine consists of an easy-to-use quasi-Newton algorithm for finding a minimum of a function subject to fixed upper and lower bounds on the independent variables, using function values only. Other NAG routines such as E04KYF or E04KZF, which also use the gradient of the function, did not significantly improve the numerical results.

Example 4.1

In order to test the accuracy, convergence and stability of the numerical solution of the inverse problem we consider first a benchmark test example for which an analytical solution for a single uniform layer is available as given by

$$n(x) \equiv n_1, \quad u(x) = \frac{2n_0 n_1 cosh(i\beta n_1(1-x)) - 2n_0 n_s sinh(i\beta n_1(1-x))}{n_1(n_0+n_s)cosh(i\beta n_1) - (n_1^2 + n_0 n_s)sinh(i\beta n_1)}, \quad x \in (0,1). \tag{34}$$

From (28) and (34), the energy reflection coefficient, or reflectance, is given by

$$|R(\beta)|^2 = |u(0)-1|^2 = \frac{n_1^2(n_0-n_s)^2 cos^2(\beta n_1) + (n_1^2 - n_0 n_s)^2 sin^2(\beta n_1)}{n_1^2(n_0+n_s)^2 cos^2(\beta n_1) + (n_1^2 + n_0 n_s)^2 sin^2(\beta n_1)}. \tag{35}$$

The phase is given by

$$\phi(\beta) := arg(R(\beta)) = tan^{-1}\left[\frac{n_0 n_1(n_1^2 - n_s^2)sin(2\beta n_1)}{n_1^2(n_0^2 - n_s^2)cos^2(\beta n_1) - (n_1^4 - n_0^2 n_s^2)sin^2(\beta n_1)}\right]. \tag{36}$$

Both the quantities (35) and (36) are shown in Figure 4 for various values of the constant $n_1 \in \{1.12, 1.23, 1.27\}$. The thickness of the slab is $d = 122nm$ (in nanometres) and $M = 46$ values of the wavelength λ_l are chosen in the interval $[350nm, 800nm]$ by taking $\beta_{min} = 2\pi d/800$ and $\beta_{max} = 2\pi d/350$ in expression (31). Note that $R(\beta) = |R(\beta)|exp(i\phi(\beta)) = |R(\beta)|cos(\phi(\beta)) + i|R(\beta)|sin(\phi(\beta))$. Notice that when $n_1 = \sqrt{n_0 n_s} \approx 1.23$, the reflection coefficient (35) can become zero for $\lambda = 2\pi d/\beta = 4dn_1$. For $n_1 \in \{n_0, n_s\}$ we obtain that $|R(\beta)| = (n_s - n_0)/(n_s + n_0)$ is independent of β. Also, when $n_1 = n_0$, $\phi(\beta) = 2\beta$, whilst when $n_1 = n_s$, $\phi(\beta) = 0$. In Figure 4, experimentally measured data for the reflectance supplied by the company Oxford Advanced Surfaces Group Plc are also included. From this figure it can be seen that this experimental data cannot in fact correspond to a simple uniform coating with constant index of refraction. Trials with piecewise constant functions, i.e. layered coatings, did not produce significantly better agreement with the experiment. Instead, as we shall see in Example 4.2, a significantly better fit is obtained by considering continuously varying spacewise-dependent indices of refraction. In order to validate the accuracy of the FDM direct solver, Figure 2 shows the numerical results obtained with various mesh sizes $h \in \{0.05, 0.1, 0.2\}$ for the percentage of reflectance $\%|R(\beta)|^2$ and the angle $\phi(\beta)$ in comparison with the exact solutions (35) and (36), when $n_1 = 1.27$. From this figure it can be seen that the numerical FDM results converge to the corresponding exact solutions (35) and (36), as

the mesh size h decreases to zero. Furthermore, it can be observed that the mesh size $h = 0.05$, corresponding to $N = 20$, is sufficiently fine in order to ensure a very good accuracy of the numerical results. Note that in the inverse problem the direct solver is called many times and therefore, there are serious computational time limitations involved in order to make the approach feasible. Hence, it is very useful if we can take a larger mesh size without affecting the accuracy of the numerical results. In all the inversion results that follow we have used $N = 20$. From eqns. (28) and (34) we

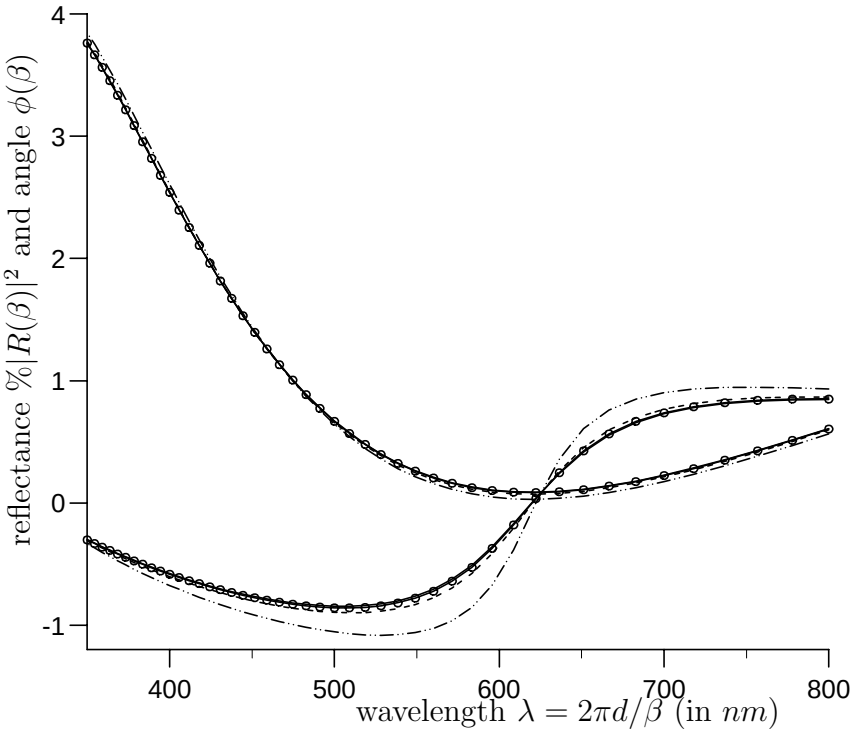

Figure 2: *The numerical FDM results obtained with various mesh sizes* $h = 0.05(- \circ -)$, $h = 0.1(- - -)$ *and* $h = 0.2(-..-)$ *for the reflectance* $\%|R(\beta)|^2$ *(upper curves) and the angle* $\phi(\beta)$ *(lower curves) in comparison with the exact solutions (35) and (36) shown with continuous lines (—), when* $n_1 = 1.27$.

also obtain that the (complex) reflection coefficient is given by

$$R(\beta) = u(0) - 1 = \frac{n_1^2(n_0 - n_s)^2 cos^2(\beta n_1) - (n_1^4 - n_0^2 n_s^2) sin^2(\beta n_1) + i n_0 n_1 (n_1^2 - n_s^2) sin(2\beta n_1)}{n_1^2(n_0 + n_s)^2 cos^2(\beta n_1) + (n_1^2 + n_0 n_s)^2 sin^2(\beta n_1)}. \quad (37)$$

Once the accuracy of the direct solver has been validated, we can now proceed to solve the inverse problem. Numerical results for the index of refraction $n(x)$ obtained by minimizing the functional

(32), based on the additional data containing the full complex reflection coefficient $R(\beta)$ given by eqn.(37), are shown in Figure 3 for various regularization parameters $\Lambda \in \{10^{-6}, 10^{-5}, 10^{-4}\}$. The initial guess is taken as the prior estimate $\underline{\epsilon}^* = \underline{1.12^2} = \underline{1.2544}$. The exact solution is the constant function $n(x) \equiv n_1 = 1.27$. There is already numerical noise introduced in the exact data (37), which can be calculated from the residual of Figure 2. The numerical value of the square of this residual calculated from Figure 2 for $h = 0.05$ is given by

$$\eta := \sum_{l=1}^{M} |u(0; \beta_l, \underline{n_1}) - 1 - R_l|^2 = 3.6E - 5. \tag{38}$$

To determine the regularization parameter Λ in (32) we can apply the discrepancy principle and choose the value of Λ for which the residual

$$\sum_{l=1}^{M} |u(0; \beta_l, \underline{\epsilon}) - 1 - R_l|^2 \approx \eta. \tag{39}$$

of the minimized functional (32) becomes approximately equal to the noise level η. For the synthetic Example 4.1, the value of η is available and the discrepancy principle can be used. However, for Example 4.2 the value of the noise level η is not available and then, more heuristic choices of the regularization parameter Λ, such as the L-curve criterion, needs to be employed. From Figure 3 it can be seen that regularization is necessary, otherwise for Λ too small, see results for $\Lambda = 10^{-6}$, an unstable least-squares solution is produced. A value of Λ between 10^{-5} and 10^{-4} is appropriate to ensure that a stable and reasonably accurate solution is obtained. The numerical results are slightly less accurate near the boundary $x \in \{0, 1\}$. This is expected due to the end effects which are well-known to decrease the convergence and accuracy of the numerical results.

Next we investigate Example 4.1 for limited additional data, as given by just the amplitude measurement (35) of the data $|R_l|$ for $l = \overline{1, M}$. We then minimize the functional (33). Numerical results obtained from this minimization are also included with markers on in Figure 3. From these results it can be clearly seen that, for Example 4.1, the limited amplitude data is not enough to produce a unique retrieval of the index of refraction, and additional information is required. On the other hand, the use of the complete information provided by the full complex reflection coefficient enables a unique retrieval of the index of refraction, as was expected from the uniqueness analysis described in Section 3.

Once the numerical method and solution have been validated in terms of accuracy and stability for the benchmark test Example 4.1, the technique is next applied in Example 4.2 to a case study concerning inverting real reflectance data supplied by the company.

Example 4.2 *(Inversion of real data)*

The data is shown by continuous line (——) in Figure 4. From the practical experiment we have available an additional phyical measurement of the full integrated refraction index (IRI)

$$1.27 = \overline{n} = \int_0^1 n(x)dx = \int_0^1 \sqrt{\epsilon(x)}dx. \tag{40}$$

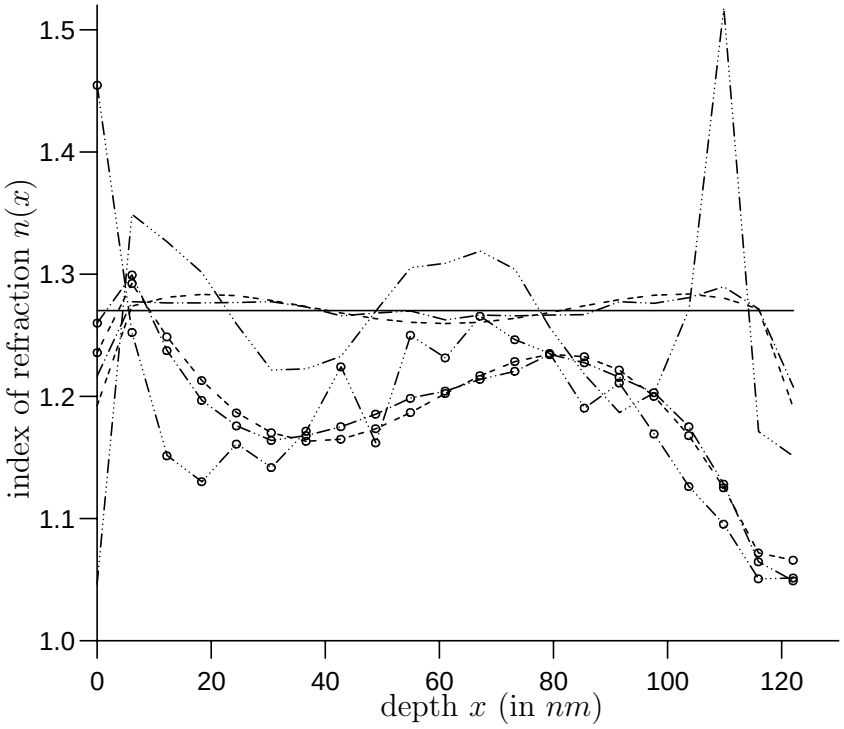

Figure 3: *The numerically retrieved refractive index profiles $n(x)$, as a function of $x \in [0, d = 122nm]$, in comparison with the exact value $n_1 = 1.27$ shown by continuous horizontal line (——), obtained with various regularization parameters $\Lambda = 10^{-6}(-....-)$, $\Lambda = 10^{-5}(-..-)$ and $\Lambda = 10^{-4}(- - -)$. The additional data is the full complex reflection coefficient $R(\beta)$ given by eqn.(37) for the curves without markers, and the limited square root of reflectance data $|R(\beta)|$ given by eqn.(35) for the curves with markers on.*

Assuming also that $n \in C[0,1]$ is a continuous function in the compact interval $[0,1]$, we have the additional constraints corresponding to an unbounded layer, namely

$$1 = n_0^2 = \epsilon(0) = \epsilon_0, \quad 1.6129 = n_s^2 = \epsilon(1) = \epsilon_N. \tag{41}$$

Although achieving a value of unity for $\epsilon(0)$ at the film-air interface is not possible since there are no low index solid materials that equal the index of air, it is still possible in practice to approach unity by reducing the packing density, see [10]. However, the coating becomes less dense and rugged as its index of refraction approaches unity. We report that instead of $\epsilon_0 = 1$ we have also tested the

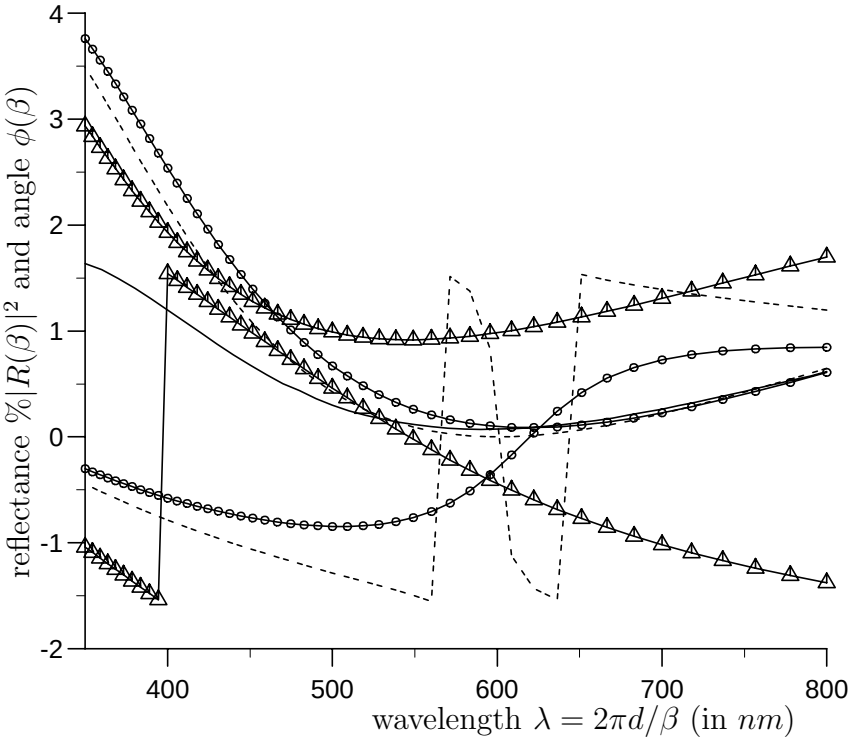

Figure 4: *The experimentally (——) measured percentance of reflectance data* $\%|R(\beta)|^2$ *and the exact solutions (35) and (36) for homogeneous single layer coatings of various constant indices of refraction* $n(x) \equiv n_1 = 1.12(-\Delta-)$, $1.23(---)$ *and* $1.27(-\circ-)$. *Reading down the intercepts with the vertical axis, the upper group of 3 marked curves corresponds to* $\%|R(\beta)|^2$, *whilst the lower group of 3 marked curves corresponds to* $\phi(\beta)$.

constraint $\epsilon_0 = 1.12^2$ corresponding to a semi-bounded layer, but the behaviour of the numerical results was not significantly different. With the *a priori* physical information (40) and (41) we thus minimize the modified functional $\tilde{F}_\Lambda : [n_0^2, n_s^2]^{N-1} \to \mathbb{R}_+$ defined by

$$\tilde{F}_\Lambda(\underline{\epsilon'}) := \sum_{l=1}^{M} ||u(0;\beta_l,\underline{\epsilon'}) - 1| - |R_l||^2 + \left[\frac{h}{2}\left(\sqrt{\epsilon_0} + \sqrt{\epsilon_N} + 2\sum_{j=1}^{N-1}\sqrt{\epsilon_j}\right) - 1.27\right]^2 + \Lambda \sum_{j=1}^{N-1}(\epsilon_j - \epsilon_j^*)^2, \qquad (42)$$

where $h = 1/N = 1/20 = 0.05$, $\underline{\epsilon'} = (\epsilon_j)_{j=\overline{1,(N-1)}} \in [n_0^2, n_s^2]^{N-1}$, and the trapezoidal rule has been employed to approximate the integral in (40); smoother constraints can be employed if one assumes

higher regularity for $n(x)$ such as $n \in C^1[0,1]$, and then one has to replace the last term in (42) by $\Lambda \sum_{j=1}^{N}(\epsilon_j - \epsilon_{j-1})^2$. The measured reflectance data is recorded at $M = 46$ uniform stations taken

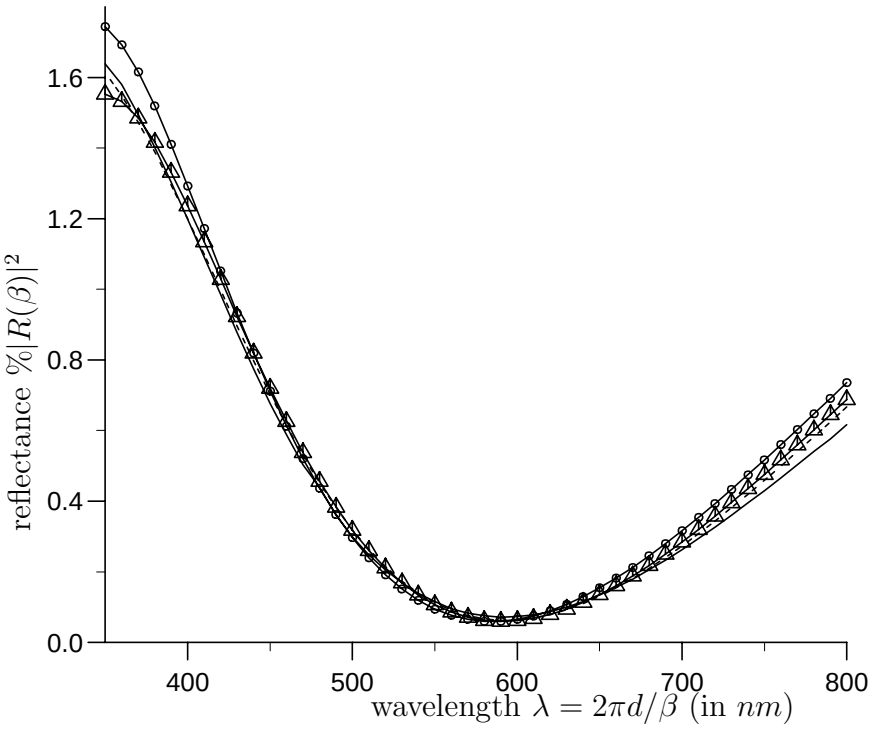

Figure 5: *The numerical results for the regularized fit of the reflectance $|R(\beta)|$ obtained with various regularization parameters $\Lambda = 10^{-5}(---)$, $\Lambda = 10^{-4}(-\Delta-)$ and $\Lambda = 10^{-3}(-\circ-)$, in comparison with the measurement data shown with continuous line (——).*

in the interval $[350nm, 800nm]$, i.e. $\lambda_l = 800 - 450(l-1)/(M-1)$, $\beta_l = 2\pi d/\lambda_l$ for $l = \overline{1,M}$. The thickness of the optical coating measured by cross-sectional scanning electron microscopy (SEM) is $d = 122nm$. The initial guess is taken as the prior estimate $\underline{\epsilon'}^* = \underline{1.27^2} = \underline{1.6129}$. Numerical results obtained for various regularization parameters $\Lambda \in \{10^{-5}, 10^{-4}, 10^{-3}\}$ are shown in Figures 5 and 6. In Figure 5, there are the results for the best fit of the reflectance $|u(0;\beta_l,\underline{\epsilon'}) - 1|$ in comparison with the measurement data $|R_l|$ for $l = \overline{1,M}$. In Figure 6, there are the numerical results for the index of refraction $n(x)$, as a function of the depth x (in nm). Again, near the ends of the slab $x \in \{0,d\}$ the results are inaccurate. By comparing Figures 4 and 5 it can be seen that a better fit of the experimentally measured reflection data is obtained when we seek a continuously varying index of refraction shown in Figure 6 than when this coefficient is sought as a piecewise

constant function. Although the fit seems to improve as Λ becomes smaller, the instability in the numerical solution increases. This is to be expected since the well-known least-squares solution obtained by taking $\Lambda = 0$ is unstable and physically meaningless although the fit to the input data is excellent. In addition, there may be issues related to the non-uniqueness of solution when using the reflectance data only as input, as discussed in Example 4.1. From Figure 6, it seems that any

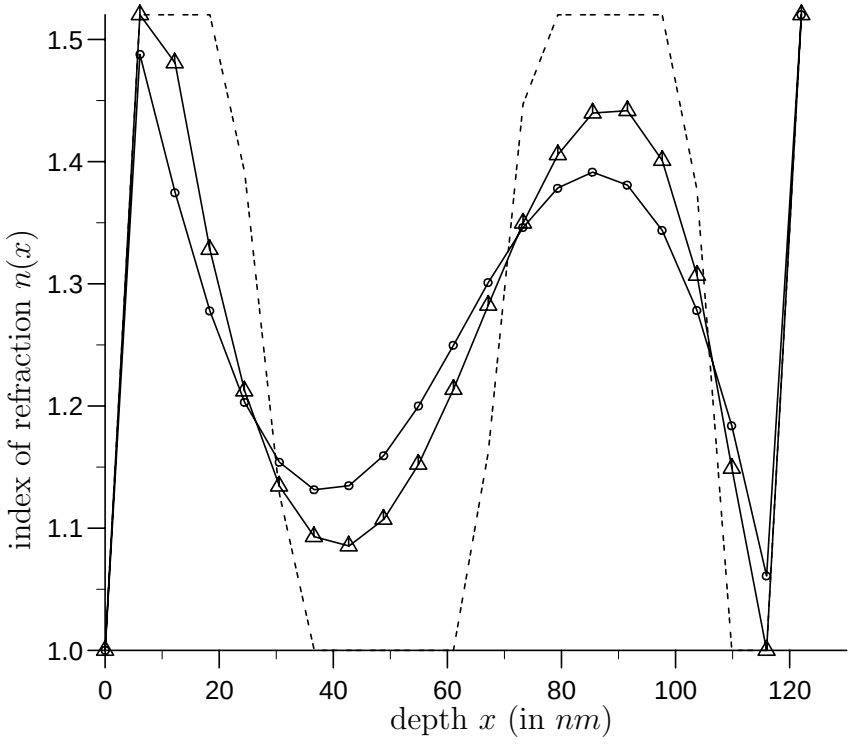

Figure 6: *The refractive index profiles $n(x)$, as a function of $x \in [0, d = 122nm]$, obtained with various regularization parameters $\Lambda = 10^{-5}(- - -)$, $\Lambda = 10^{-4}(-\Delta-)$ and $\Lambda = 10^{-3}(- \circ -)$.*

of the solutions obtained with the various regularization parameters $\Lambda \in \{10^{-5}, 10^{-4}, 10^{-3}\}$ could be taken as a good candidate for the true unknown value of the index of refraction. In order to make some choice and decide on a suitable compromise we plot the L-curve, i.e. the norm of the solution

$$Solution\ norm := ||\underline{\epsilon}' - \underline{\epsilon}'^*||$$

versus the residual

$$Residual := \sqrt{\tilde{F}_\Lambda(\underline{\epsilon}') - \Lambda||\underline{\epsilon}' - \underline{\epsilon}'^*||^2}.$$

This L-curve plot is shown in Figure 7. As expected, the portion to the right of the curve corresponds to over-smoothed solutions characterised by large values of Λ, whilst the portion to the left of the

curve corresponds to under-smoothed unstable solutions characterised by small values of Λ. The compromise that the L-criterion suggests is to select the regularization parameter Λ corresponding to the corner of the L-curve where the over- and under-smoothed portions meet. From Figure 7, it can be seen that such an L-corner corresponds to a value of $\Lambda \approx 10^{-4}$. Therefore, the curve marked with triangles $(-\Delta-)$ in Figure 6 corresponding to this value of $\Lambda = 10^{-4}$ is recommended as a good stable approximation of the index of refraction for Example 4.2.

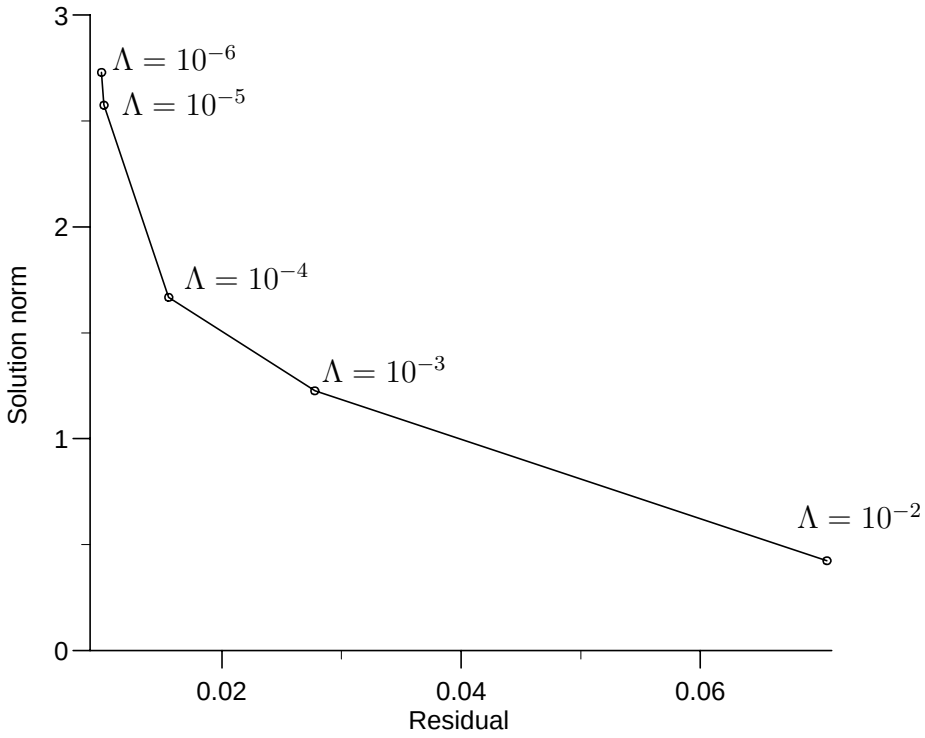

Figure 7: *The L-curve plot of the solution norm versus the residual for various values of* Λ.

5 Conclusions

In this maths-in industry case study, the determination of the index of refraction of anti-reflection coatings has been attempted. The additional data necessary for the inversion can be the full complex reflection coefficient or its absolute value only, measured for many wavenumbers. The numerical method was based on a finite-difference direct solver combined with a nonlinear Tikhonov regularization procedure. The choice of the regularization parameter was based on the discrepancy principle or the L-curve criterion. The need to use both the real and imaginary parts of the complex reflection coefficient in order to render a unique solution has been investigated in Section 3 and in

Example 4.1 of Section 4. It was shown that, in general, the knowledge of the full complex reflection coefficient is necessary to determine uniquely a spacewise continuous index of refraction. When only the absolute value of the reflection coefficient is used as input data, constraints need to be imposed, for example, the knowledge of the full integrated refraction index, additional smoothness assumptions on the index of refraction, or more reflectance data measured for many wavelengths. Also, the use of additional reflectance data at non-normal incidence, see [18] and [23], the finite-dimensional parameterisation of the unknown coefficient using cubic splines or the piecewise constant layered material assumption could be useful ideas to reduce the non-uniqueness of solution of the inverse problem. Furthermore, the practical measurement by the company QinetiQ Malvern Ltd. of the phase shift $\phi_l := arg(R_l)$ for $l = \overline{1, M}$, is at present ongoing using a combination of modulated reflectance spectroscopy, X-ray reflectivity and modulated interferometry, see [20].

Apart from this insight into the uniqueness of solution of the inverse problem, our principal conclusion is that, as shown in Figure 5, a better fit of the reflectance measured data is obtained by using a continuously varying index of refraction (see Figure 6 for $\Lambda = 10^{-4}$) than when this coefficient is sought as piecewise constant function, as in previous studies.

Acknowledgements

The authors would like to thank the University of Leeds Enterprise Knowledge Transfer (EKT) and the UK Knowledge Transfer Network (KTN) for Industrial Mathematics whose partial funds facilitated some meetings between the academic and the industrial partners. The industrial partner G. Wakefield would also like to thank the Technology Strategy Board (TSB) for partial funding related to the research undertaken in this paper. Aspects of this work have also been presented at the *4th Industrial Inverse Problems Sandpit* held between 22nd-23rd March 2010 at the University of Leeds. The comments and suggestions made by the referee are gratefully acknowledged.

References

[1] O.V. Belai, L.L. Frumin, E.V. Podivilov, and D.A. Shapiro, *Inverse scattering for the one-dimensional Helmholtz equation: fast numerical method*, Optics Letters **33** (2008), 2101–2103. 159, 160

[2] K. Chadan and P.C. Sabatier, *Inverse problems in quantum scattering theory, 2nd. ed.*, Springer-Verlag, Berlin, 1989. 159, 161

[3] M.J. Chaubell, *Low-coherence interferometric imaging: Solution of the one-dimensional inverse scattering problem*, Ph.D. thesis, California Institute of Technology, 2004. 159

[4] D. Chen, *Anti-reflection (AR) coatings made by sol-gel process: A review*, Solar Energy Materials and Solar Cells **68** (2001), 365–391. 155

[5] Y. Chen and V. Rokhlin, *On the inverse scattering problem for the Helmholtz equation in one dimension*, Inverse Problems **8** (1992), 365–391. 159

[6] P. Deift and E. Trubowitz, *Inverse scattering on the line*, Communications on Pure and Applied Mathematics **32** (1979), 121–251. 161

[7] V.I. Dmitriev and A.S. Chernyavskii, *Integral characteristic method in the inverse problem of optical coating design*, Computational Mathematics and Modelling **12** (2001), 128–136. 158, 159

[8] M. Dunn and S.I. Hariharan, *Numerical computations on one-dimensional inverse scattering problems*, Tech. Report 166114, NASA Contractor Report, 1983. 158

[9] ———, *Numerical computations on one-dimensional inverse scattering problems*, NASA Contractor Report **55** (1984), 157–165. 159

[10] T.H. Elmer and F.W. Martin, *Antireflection films and alkali-borosilicate glasses produced by chemical treatments*, American Ceramic Society Bulletin **55** (1979), 1092–1097. 166

[11] P.V. Frangos and D.L. Jaggard, *A numerical solution to the Zakharov-Shabat inverse scattering problem*, IEEE Transactions on Antennas and Propagation **39** (1991), 74–79. 159

[12] M.A. Green, *High efficiency silicon solar cells*, Trans Tech Publications, Aedermannsdorf, Switzerland, 1987. 155, 156

[13] F. Hagin, *Some numerical approaches to solving one-dimensional inverse problems*, Journal of Computational Physics **43** (1981), 16–30. 159

[14] M. Hanke, *Limitations of the L-curve method in ill-posed problems*, BIT **36** (1996), 287–301. 159

[15] P.C. Hansen, *The L-curve and its use in the numerical treatment of inverse problems*, Computational Inverse Problems in Electrocardiology, Advances in Computational Bioengineering Series, vol. 4, pp. 119–142, WIT Press, Southampton, 2001. 159

[16] V. Janicki, J. Sancho-Parramon, and H. Zorc, *Refractive index profile modelling of dielectric inhomogeneous coatings using effective medium theories*, Thin Solid Films **516** (2008), 3368–3373. 159

[17] A. Mahdjoub and L. Zighed, *New designs for graded refractive index antireflection coatings*, Thin Solid Films **478** (2005), 299–304. 159

[18] M.J. Minot, *The angular reflectance of a single layer gradient refractive-index films*, Journal of the Optical Society of America **67** (1977), 1046–1050. 171

[19] P. Nubile, *Analytical design of antireflection coatings for silicon photovoltaic devices*, Thin Solid Films **342** (1999), 257–261. 159

[20] W.J. Plieth and H. Bruckner, *Experimental determination of the complex Fresnel reflection coefficient of a three-phase system by combination of modulated reflectance spectroscopy and modulated interferometry*, Surface Science **66** (1977), 357–360. 171

[21] D. Ristau, H. Schink, F. Mittendorf, S.M.J. Akhtar, J. Ebert, and H. Welling, *laser induced damage of dielectric systems with gradual interfaces at* $1.064\mu m$, NIST Special Publications **775** (1988), 414–426. 159

[22] P. Sacks, *An inverse problem in coupled mode theory*, Journal of Mathematical Physics **45** (2004), 1699–1710. 161

[23] B. Sheldon, J.S. Haggerty, and A.G. Emslie, *Exact computation of the reflectance of a surface layer of arbitrary refractive-index profile and an approximate solution of the inverse problem*, Journal of the Optical Society of America **72** (1982), 1049–1055. 171

[24] S.M. Sze, *Semiconductor Devices*, Wiley, New York, 1985. 155

[25] P. Vukusic, *Natural photonics*, Physics World (2004), 35–39. 155

[26] G. Xiao and K. Yashiro, *An efficient algorithm for solving Zakharov-Shabat inverse scattering problem*, IEEE Transactions on Antennas and Propagation **50** (2002), 807–810. 159

[27] J. Zhao and M.A. Green, *Optimized antireflection coatings for high-efficiency silicon solar cells*, IEEE Transactions on Electron Devices **38** (1991), 1925–1934. 156, 159